ADVANCED FUNCTIONAL MATERIALS
www.afm-journal.de

Direct Ionic Ink Writing on and Penetrating into Elastomer for Patternable, Waterproof, and Wear-Resistant Ionic Circuits

*Yao An, Junshi Wu, Beihang Xu, Jinghao Zhu, Antong Ma, Wenjin Wang, Yongjia Yang, Xiaodong Lian, Zhaoxiang Yang, Yapei Wang, and Yonglin He**

The increasing need for ionic circuits has driven the demand for patterning methods with excellent wear resistance and ease of preparation. However, the traditional method of the circuits modified on the surface frequently suffers from wear and detachment during use. Herein, an interpenetrating network of poly(ionic liquid) and polyurethane is employed, creating a patternable ionic circuit that can resist the abrasion of sandpaper or taping. Hydrophobic ionic liquids are successfully polymerized inside the polyurethane to achieve a waterproof ionic circuit, simultaneously reducing the impact of environmental humidity. Additionally, this ionic circuit possesses the capability to perceive the multisignals of temperature, pressure, and pressing shapes with the assistance of artificial intelligence. The interpenetrating network provides a simple and practical solution for the fabrication of wear-resistant and stable patterned ionic circuits.

1. Introduction

The ionic conductor has emerged as an important material for the Human-Computer Interface (HCI) due to its inherent advantages,[1] including flexibility,[2,3] transparency,[4,5] biocompatibility,[6] and resistance to magnetic interference.[7] In specific HCI applications like smart healthcare,[8] smart sports,[9,10] and smart homes,[11–14] there has been increasing demand for the integration of diverse functionalities. Precise patterning techniques[15–18] are important in function integration,[19–21] which enables the control of circuit structures and layouts and facilitates the collaboration of various modules and the development of sophisticated applications. Additionally, patterning also plays a critical role in device miniaturization,[22] enhancing performance while reducing inter-circuit interference and losses. Furthermore, custom-designed circuits created through patterning techniques can drive the adoption of wearable devices for medical and health monitoring purposes.

Unlike traditional integrated circuit manufacturing, the focus on patterned technology for ionic conductors underscores the importance of wear resistance. Given that HCI functionality often involves frequent direct contact with objects, which may lead to friction altering the properties of the ionic circuit or causing circuit breakage, the development of a robust wear-resistant patterning method is indispensable for advancing the field of ionic circuits.

Currently, the primary techniques for patterning ionic conductors include mask templating,[23–25] 3D printing,[26–28] and electrochemical methods.[29,30] Flexible porous or reactive substrate materials are revolutionizing flexible circuits with their unique physical properties and chemical compatibility. In particular, substrates such as paper, fabrics, electrospun nanofibres, and natural porous materials are favored for their lightness, breathability, and biocompatibility. Combined with conductive inks such as metal nanoparticles, carbon-based materials, and conductive polymers, the synergistic effect between these functional inks and the substrate materials helps us to design flexible circuits with better performance.[24] Nevertheless, the resulting patterned circuits frequently protrude from the substrate surface, rendering them vulnerable to abrasion.[31] Additionally, widely employed ionic conductors like hydrogels and organogels are often susceptible to humidity, with residual moisture from object contact potentially compromising their electrical precision.[32,33] An immediate requirement exists for a straightforward, durable, and wear-resistant patterning approach for stable ionic circuits.

Herein, we have developed a straightforward technique for patterning ionic circuits known as direct ionic ink writing (DIIW). In this method, hydrophobic ionic liquids are utilized to interpenetrate with polyurethanes. Due to the robust mechanical properties of polyurethane as a supportive substrate, it effectively shields the ionic liquid circuit within the bulk phase

Y. An, B. Xu, J. Zhu, A. Ma, W. Wang, Y. Yang, X. Lian, Z. Yang, Y. Wang, Y. He
Key Laboratory of Advanced Light Conversion Materials and Biophotonics
School of Chemistry and Life Resources
Renmin University of China
Beijing 100872, China
E-mail: heman@ruc.edu.cn
J. Wu
Huangpu Institute of Materials
Guangzhou 510530, China

The ORCID identification number(s) for the author(s) of this article can be found under https://doi.org/10.1002/adfm.202413434

DOI: 10.1002/adfm.202413434

from abrasion. Furthermore, hydrophobic ionic liquids exhibit high resistance to ambient moisture, ensuring the stability of the electrical signal. The resultant patterned ionic circuits produced through DIIW offer the potential for multi-signal monitoring and recognition in tandem with artificial intelligence (AI).

2. Results and Discussion

2.1. Materials Preparation and Characterization

The procedure of the direct ionic ink writing (DIIW) and the formation of the interpenetrating networks comprising polyurethane (PU) and poly(ionic liquids) (PILs) are illustrated in **Figure 1**a. The PU was synthesized through a one-step polymerization involving poly(propylene glycol) (PPG), hexamethylene diisocyanate (HDI), and 1,3,5-Tris(6-isocyanatohexyl)-1,3,5-triazinane-2,4,6-trione (THDI) (Figure S1 and S2, Supporting Information). The tensile curves of PU with different functionalities (*f*, Figure 1b) were determined, and the results for elongation at break and Young's modulus are presented in Figure 1c. It is evident that Young's modulus increases progressively with higher functionalities and crosslinking, while elongation at break decreases. The PU with the *f* of 2.18 was chosen for subsequent experiments unless specified otherwise, as it exhibits comparable modulus and elongation at break properties.

The ionic liquid solution (ILS) consisting of 1-hexyl-3-vinylimidazolium hexafluorophosphate ([HVIm][PF_6]), 1-allyl-3-vinylimidazolyl hexafluorophosphate ([AVIm][PF_6]), photoinitiator and dichloromethane was used as ink. The [HVIm][PF_6] and the [AVIm][PF_6] were synthesized based on previous work[34] and confirmed by ^{1}H NMR (Figure S3, Supporting Information) and FT-IR (Figure S4, Supporting Information) spectra. It is noteworthy that [HVIm][PF_6] is soluble in PPG, a characteristic believed to enhance the compatibility of the interpenetrating networks and solubility of ions[35] (Figure S5, Supporting Information). Moreover, ^{1}H NMR (Figure S6, Supporting Information) and FT-IR (Figure S7, Supporting Information) spectra indicate that hydrogen bonds are formed between the ionic liquid and the polyurethane, which further enhances ionic mobility. Upon exposure to UV light, [HVIm][PF_6] could be polymerized into PILs networks with the crosslinker of [AVIm][PF_6], which also has been validated by ^{1}H NMR spectra (Figure 1d; Figure S8, Supporting Information).

Before polymerization, the ILS could swell the PU with the assistance of the dichloromethane. The mass swelling ratio of the PU immersed in the ILS has been measured and provided in Figure 1e, which indicates that the swelling of PU by ILS was saturated at the fourth hour. The ILS-swollen PU was then treated in a vacuum oven at the eighth hour, and the dichloromethane was nearly completely removed within 3 h. In the subsequent experiments, a standard protocol involved a 6-h swelling period at 20 °C, followed by vacuum oven treatment at 80 °C for 8 h to ensure complete removal of the dichloromethane solvent. A fluorescence microscope has been used to observe the penetration process of ionic ink in the polyurethane substrate, which provides dynamic information on this process (Figure S9, Supporting Information).

After removing the solvent, the ILs are polymerized under UV light to form a PU-ILs interpenetrating network. It could be noted that the ILs remained transparent and soft after polymerization in the PU (Figure 1f). Crucially, the polymerized ILs were hydrophobic, indicating potential as ionic circuits that are not susceptible to ambient humidity (Figure 1g). It is worth mentioning that the pink hue of the ILs is attributed to the inclusion of the dye rhodamine B. Comparison of the Differential Scanning Calorimetry (DSC) curves proved that the PILs network could slightly decrease the T_g and may act as a plasticizer (Figure S10, Supporting Information). The rheological behavior of different chemical compositions and the mechanical properties of PILs-interpenetrated PU (PIL-PU) at different temperatures were also measured (Figure S11, Supporting Information).

2.2. Patterned Methods

The prepared ink could be patterned in the substrate by various methods (Figure S12, Supporting Information). As shown in **Figure 2**a, the ionic ink could be directly written on the PU, and patterns, including Chinese characters, English letters, figures, and lines, are applicable with a brush (Figure 2d). In addition, patterns could be also created by stamps (Figure 2b), and clear outlines of the characters and figures are shown in Figure 2e. Stamps offer the potential for mass production of ionic circuits while hand-writing remains the simplest method for creating such circuits. Alternatively, patterns could be printed by an inkjet printer (Figure 2c). Using the printheads with diameters of 50 and 80 μm, the inkjet printer produces two straight lines with diameters of 20 and 100 μm, respectively (Figure 2f, left column). The sizes are different from that of the printhead due to slight ink spreading over the PU and trace shrinking during dichloromethane evaporation. It should be noted that precise patterns could be also made by writing (Figure 2f, right column). The rectangles of handwriting have sharp angles, and the number "1" has a length of ≈230 μm and a width of ≈140 μm. The minimum width of a handwritten line is ≈40 μm, which is the limit of visibility to the naked eye. Most importantly, the polymerized ionic patterns remain flexible (Figure S13, Supporting Information).

The cross-section of the pattern and the formation of the interpenetrating network are investigated by fluorescence microscope, SEM, and EDS. As shown in Figure 2g, a straight line was written on the PU with the ionic ink. After polymerization, the cross-section was observed by the fluorescence microscope, and it showed that the ionic liquids (ILs) penetrated the PU to form a semicircular diffusion region under the surface. The diffusion depth was ≈500 μm. EDS images of the cross-section prove that the elements of fluorine (Figure 2j) and phosphorus (Figure 2k) associated with ILs are also distributed in the semicircular diffusion region (within the white dashed line, Figure 2i). Besides, the EDS spectra of the non-ink Zone I and the ink Zone II in Figure 2h were compared, confirming the existence of elements fluorine and phosphorus (Figure 2h).

2.3. Wear-resistance and Waterproofness of Ionic Circuits

The mechanism of the ionic conduction could belong to the electrolyte-swollen ionic transport model.[35] To provide the

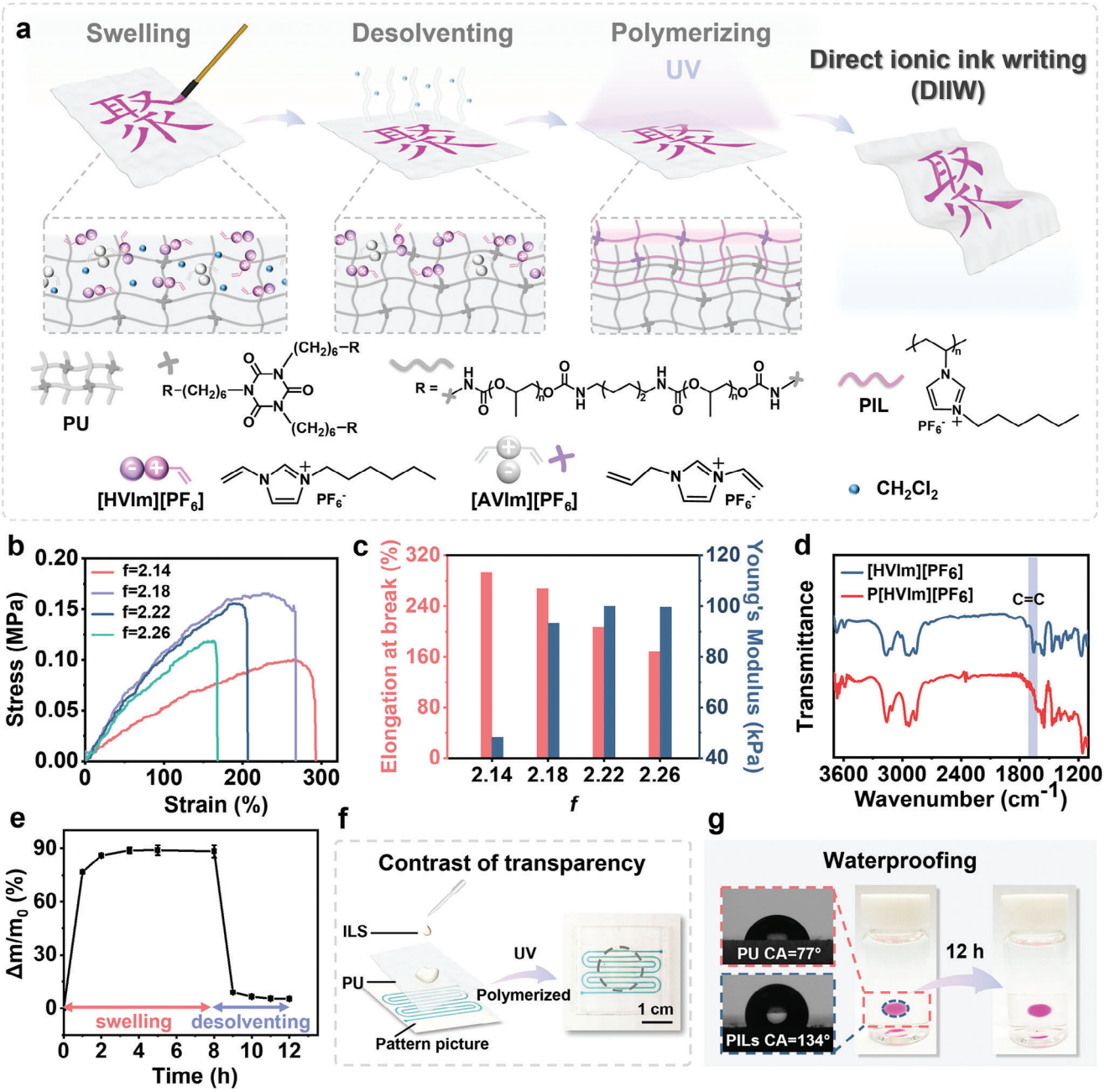

Figure 1. a) Schematic illustration of the direct ionic ink writing (DIIW) and the formation of the interpenetrating networks based on polyurethane (PU) and ionic liquid. b) Stress-strain curves of PU with different functionality. c) Comparison of Young's modulus and elongation at break of PU with different functionality. d) FT-IR spectra of the poly(ionic liquids) (PILs) before and after polymerization. e) Swelling and desolventing curves of PU in ILS. f) Comparison of the transparency of PU and PILs-interpenetrated PU. The serpentine circuit is on the paper under the PU, and the area within the circle of the dashed line is PILs-interpenetrated PU. g) Photographs of PILs-interpenetrated PU before and after immersing in water for 12 h. The insets are photographs of the contact angles of water droplets on the surfaces of PU and PILs-interpenetrated PU.

equivalent circuit of the ion transport and quantitive data on the conductivity, the Nyquist plot and the Bode phase plot have been shown and discussed in Figure S14 (Supporting Information). Additionally, a piece of PILs-interpenetrated PU has been integrated into an electrical circuit as Figure S15 (Supporting Information). These provide direct evidence that the ionic circuit possesses conductive properties. The conductivity of PIL-PU with curing time, different dichloromethane contents, and temperature are also discussed[36] (Figures S16–S18, Supporting Information).

The wear resistance of the patterned ionic circuits has been evaluated. As shown in **Figure 3**a, repeated abrasion of patterned ionic circuits has been conducted on the sandpaper. Specifically, the ionic circuit was fixed to the bottom of a 500 g weight

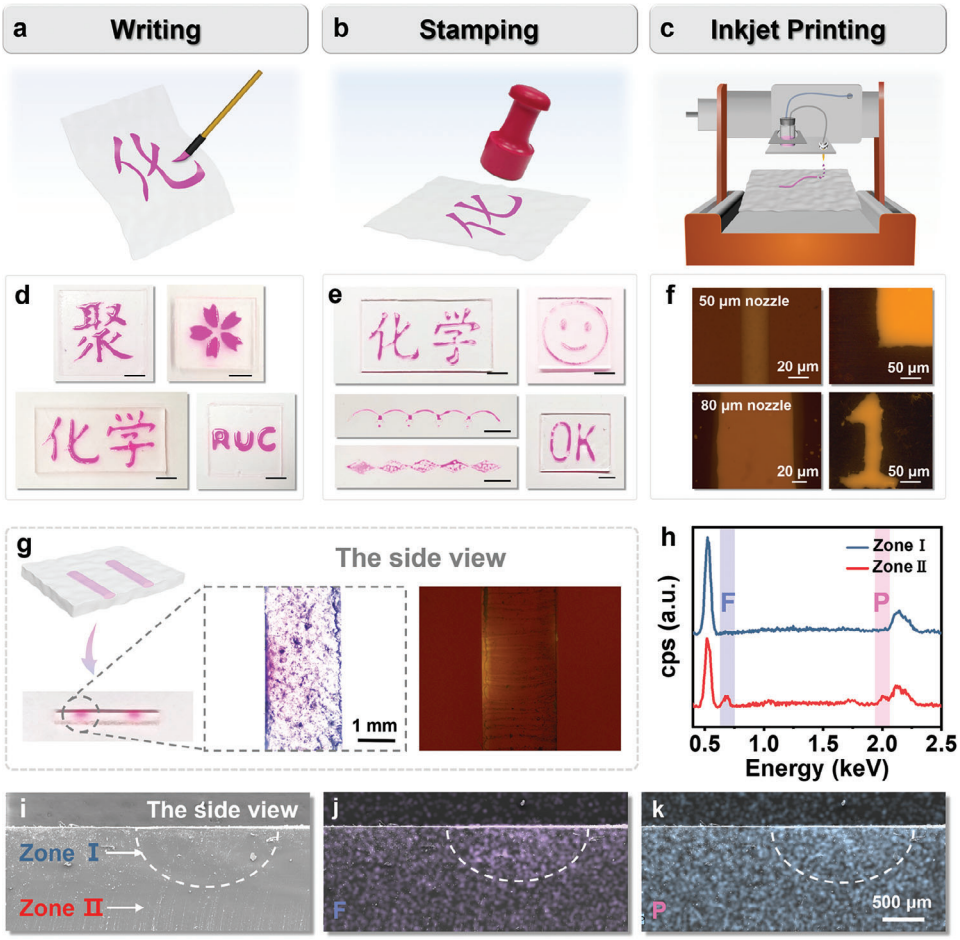

Figure 2. a–f) Illustrations and optical photographs of patterns prepared by writing (a,d, and the left column of f), stamping (b,e), and inkjet printing (c and the right column of f). Black scale bar: 5 mm. g) The cross-section of the ionic circuit and its optical images of ordinary microscope and fluorescence microscope. h) EDS intensities of fluorine and phosphorus in Zone I and Zone II. i–k) SEM and EDS images of the cross-section.

and then dragged to 30 cm. The results indicate that the R/R_0 remained almost stable even after 10 times abrasion. It is believed that the abrasion only damages a relatively thin layer of the PU surface (Figure S19, Supporting Information), and the interpenetrating network of PILs and PU is deep enough to withstand the effects of abrasion. Additionally, the damage of sandpaper abrasion to the ionic circuits was analyzed using SEM and EDS (Figure 3c,d). The SEM images indicate that the surface of the PU became rough after abrasion while the EDS intensities confirm the existence of fluorine and phosphorus elements before and after abrasion (Figure 3e,f). Therefore, the ionic circuit could be conductive even after cycles of abrasion. A more visible comparison has been provided in Figure S20 (Supporting Information), in which a DC power supply, the ionic wire, and a green light-emitting diode (LED) were connected. It was observed that the green LED could be lit up before and after the abrasion of the sandpaper. Moreover, repeated taping and tearing off of 3 M tape on the ionic circuits has also been used to assess its robustness. Little changes in the resistance have been observed after several times of tape-peeling (Figure 3b).

Waterproofing is an important requirement for the advancement of ionic circuits. The ionic circuits fabricated by DIIW have been evaluated in environments of different humidities. As shown in Figure 3g, little change has been observed on the R/R_0 of the ionic circuits under conditions of different humidities, indicating the stability of the circuits. The ionic circuits also have been immersed in water, and a vortex mixer or a magnetic stirrer has been used in this procedure. No significant change of the R/R_0 has been recorded for the ionic circuits after immersing for several hours (Figure 3h,i). It is believed that the waterproofness could be attributed to the hydrophobicity of the PU and the ionic liquid.

2.4. AI-enabled Multisignal Recognition with Patterned Ionic Network

On the basis of the straightforward patterning approach of DIIW, stable and wear-resistant ionic circuits could be prepared successfully. As a demonstration of the HCI, an ionic network has been developed to achieve multisignal recognition with AI models. The ionic network composed of three horizontal and three vertical ionic lines has 3 × 3 nodes, and it is connected to six positive electrodes (denoted as a to f) and six negative

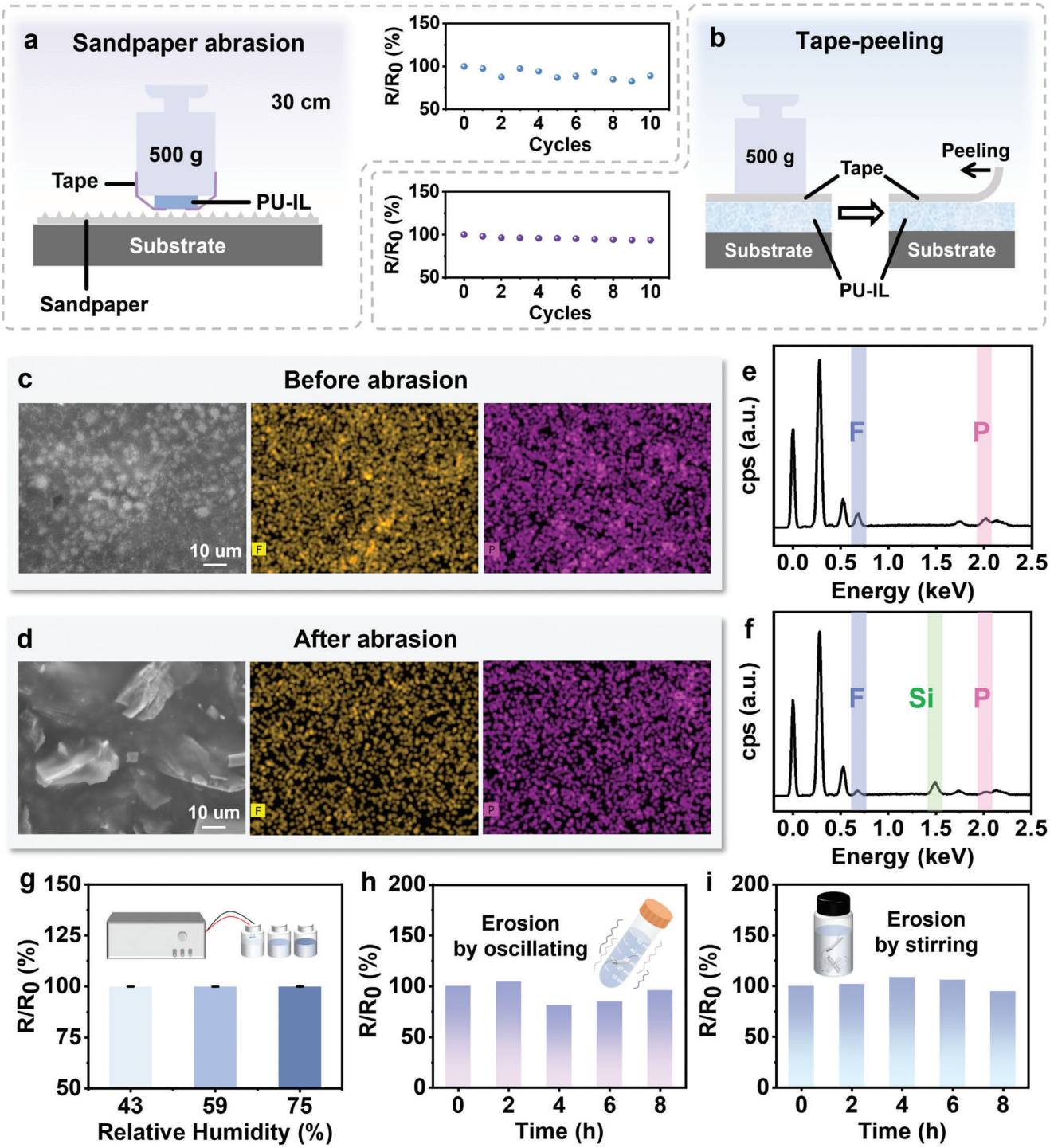

Figure 3. a,b) Diagram and resistance changes of sandpaper abrasion and tape-peeling. c,d) The SEM and EDS images of the ionic circuit before and after abrasion. e,f) The intensities of elements fluorine and phosphorus before (e) and after (f) sandpaper abrasion. g) Electrical stability of the ionic circuits under conditions of different humidities. h,i) Resistance changes of the ionic circuit under the erosion of water by oscillating and stirring.

electrodes (denoted as 1 to 6) (Figure 4b; Figure S21, Supporting information). The ionic network could perceive different kinds of signals, including temperature, pressure, and pressing shapes (**Figure** 4a,c; Figures S22 and S23, Supporting information). For each case, 36 feature values, namely 36 resistance values between positive electrodes and negative electrodes, were recorded and labeled as 1-a, 1-b, 1-c, 1-d, 1-e, 1-f, ..., 6-f. These feature values are closely associated with the signals of temperature, pressure, and pressing shapes (Figure S24, Supporting information), and they are utilized as input for machine learning.

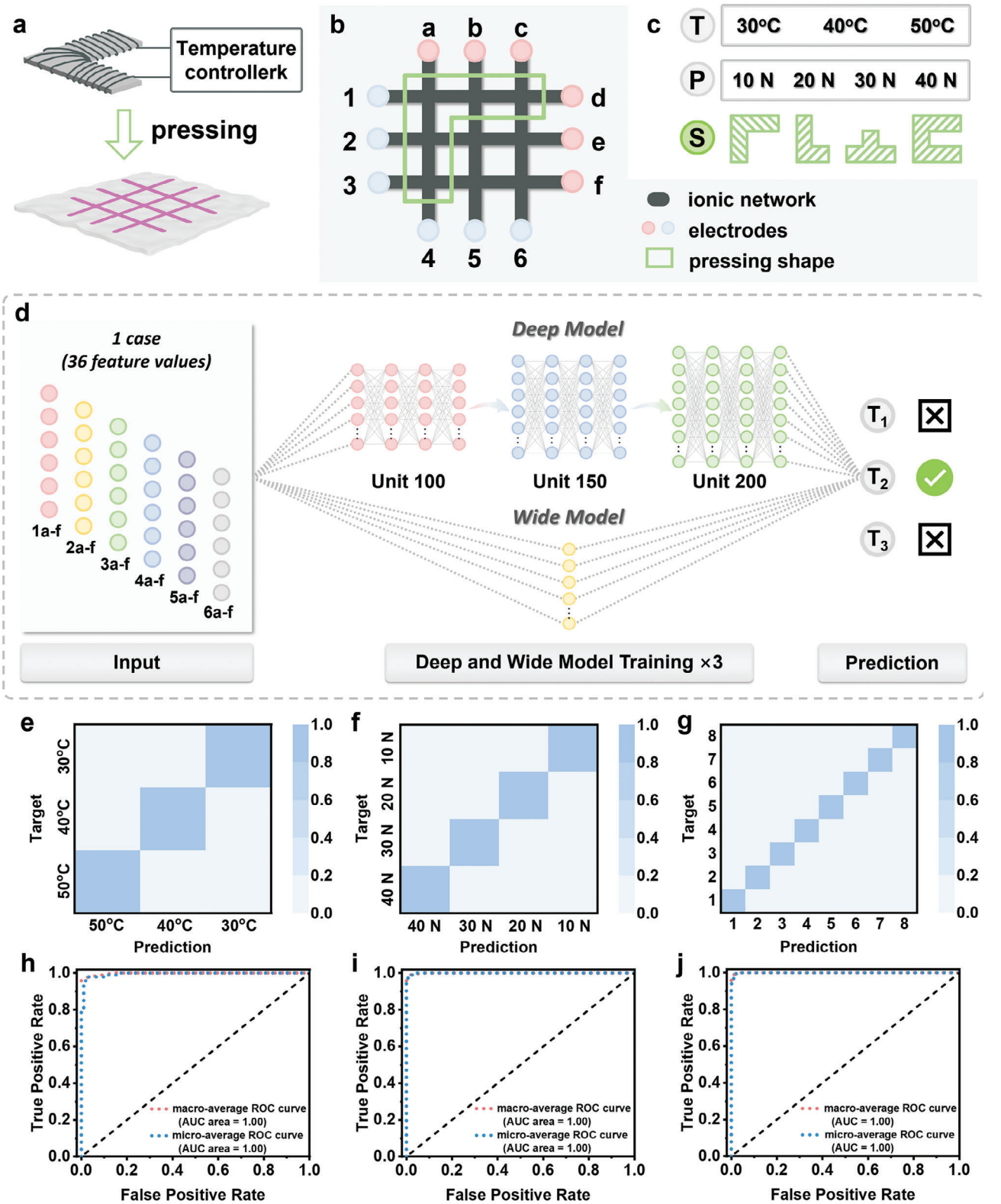

Figure 4. a,b) Schematic diagrams of the test method (a) and the ionic network with electrodes (b). c) Temperatures, pressures, and pressing shapes on the ionic network. d) Schematic diagram illustrating the procedure of electrical signal recognition at different temperatures, pressures, and pressing shapes, including signal input, model training, and prediction. e–g) Confusion matrix of classification results at different temperatures, pressures, and pressing shapes. h–j) The ROC curves and AUC areas of predictions of temperatures, pressures, and pressing shapes, respectively.

As shown in Figure 4d, a Deep & Wide model has been used in this work, in which the Deep model is designed for generalization while the Wide model works better in memorization of feature interactions.[37] This model combines the benefits of memorization and generalization, resulting in a high accuracy of prediction. Taking the temperature prediction as an example, the accuracy reached almost 100% on the training set and 94.4% on the test set after 202 epochs of training. The confusion matrix in Figure 4e confirms the high classification accuracy for each temperature. Similarly, the accuracies for both pressure and shape were close to 100% (Figure S12, Supporting Information) and their confusion matrices are provided in Figure 4f,g, separately. Additionally, a comprehensive evaluation has been conducted of the model performance by receiver operating characteristic curves (ROC) and areas under curves (AUC). As shown in Figure 4h–j, the prediction accuracy of the model remained high under different conditions, further verifying its reliability and stability in practical applications. In summary, with patterned circuits and machine learning, the ionic network could effectively recognize multisignals, and we believe it would play an important role in complex HCI applications.

Additionally, as a demonstration, the prepared ionic circuit film was directly attached to the skin of the hand, followed by patting a basketball and recording the changes in the resistance signals. After patting the ball 100 times, the electrical signals remained stable (Figure S25, Supporting information), indicating its sensing performance under such intense and frequent contact as well as humid conditions is stable.

3. Conclusion

In this research, a novel wear-resistant patterning technique for ionic circuits, known as DIIW, was introduced. The incorporation of an interpenetrating network of PILs and PU imparts significant damage resistance to the ionic circuits. The simplicity of this method allows for patterning using various approaches, including direct writing, stamping, and inkjet printing. Importantly, the abrasion assessment revealed that the ionic circuits produced through DIIW demonstrate outstanding wear resistance attributed to the interpenetrating network structure. Furthermore, these circuits exhibit insensitivity to changes in humidity, enhancing their suitability for prolonged usage compared to conventional hydrogel-based counterparts.

Moreover, the ionic network created through this method displays electrical responsiveness to external stimuli such as temperature, pressure, and shape variations, which can be perceived by machine learning. Given the progress in ionic materials and the pressing need for circuit enhancements, we anticipate that this patterning technique for ionic circuits will play an important role in advancing the field of ionic devices.

4. Experimental Section

Materials: All chemicals were used without further purification unless otherwise stated. 1-hexyl-3-vinylimidazolium hexafluorophosphate ([HVIm][PF_6]) and 1-vinyl-3-vinylimidazolyl hexafluorophosphate ([AVIm][PF_6]) were synthesized based on previous work. 2-Hydroxy-2-methyl-phenyl-propane-1-one (Irgacure 1173) was obtained from Energy Chemical (Anhui, China). Hexamethylene Diisocyanate (HDI) and 1,3,5-Tris(6-isocyanatohexyl)-1,3,5-triazinane-2,4,6-trione (THDI) were purchased from TCI (Shanghai, China). Dibutyltin dilaurate (DBTDL) and poly(propylene glycol) (PPG) were purchased from Aladdin Bio-Chem (Shanghai, China). Rhodamine B was purchased from Alfa Aesar (CI 45170).

Synthesis of [HVIm][PF_6]: First, 1-Hexyl-3-vinylimidazolium Bromide [HVIm]Br was prepared.[38] N-vinylimidazole and 1-bromohexane were used as raw materials in a molar ratio of 1.2:1, dissolved in ethyl acetate under nitrogen protection and mechanical stirring. The mixture was refluxed at 65 °C for 24 h. After cooling, the reaction mixture was washed with ethyl acetate (the volume ratio of the sample to ethyl acetate was 3:2), followed by thorough shaking on a Kjeldahl shaker for 2 min and standing for 10 min. The ethyl acetate layer was removed, and this washing process was repeated three times. The remaining liquid was then transferred to a rotary evaporator and the residual ethyl acetate was removed under reduced pressure at 80 °C. The purified liquid was transferred to a beaker and placed in a vacuum drying oven, where it was dried under vacuum at 70 °C for 36 h to obtain [HVIm]Br. The product [HVIm]Br was then mixed with potassium hexafluorophosphate (KPF_6) in a molar ratio of 1:1.2 in acetonitrile to form 1-hexyl-3-vinylimidazolium hexafluorophosphate ([HVIm]PF_6). After the ionic liquid phase was repeatedly washed with deionized water, it was transferred to a rotary evaporator. The remaining solvent was removed by reduced pressure distillation at 100 °C using a dimethyl silicone oil bath. Subsequently, the product was placed in a constant temperature drying oven at 70 °C and dried for 36 h to yield the purified [HVIm]PF_6. [HVIm]PF_6: ^{1}H NMR (400 MHz, DMSO-d6, δ) 9.45 (s, 1H), 8.17 (s, 1H), 7.91 (s, 1H), 7.25 (s, 1H), 5.95 (s, 1H), 5.42 (s, 1H), 4.17 (s, 2H), 1.81 (s, 2H), 1.27 (s, 6H), 0.85 (s, 3H).

Synthesis of [AVIm][PF_6]: First, 1-allyl-3-vinylimidazole chloride [AVIm]Cl was prepared. Typically, N-vinylimidazole and allyl chloride were used as raw materials in a molar ratio of 1.2:1 and dissolved in acetonitrile. Under nitrogen protection and with mechanical stirring, the mixture was reacted at 70 °C for 24 h. Subsequently, the excess allyl chloride was removed by rotary evaporation. The unreacted N-vinylimidazole was extracted using ethyl acetate. Finally, the product was dried in a vacuum oven to obtain [AVIm]Cl. The product [AVIm]Cl was then mixed with KPF_6 in a molar ratio of 1:1.2 in acetonitrile to form 1-allyl-3-vinylimidazolium hexafluorophosphate [AVIm]PF_6. After the ionic liquid phase was repeatedly washed with deionized water, it was transferred to a rotary evaporator. The remaining solvent was removed by reduced pressure distillation at 100 °C using a dimethyl silicone oil bath. The product was then placed in a constant temperature drying oven at 70 °C and dried for 36 h to yield the purified [AVIm]PF_6. [AVIm]PF_6: ^{1}H NMR (400 MHz, DMSO-d6, δ) ^{1}H NMR (400 MHz, DMSO-d6, δ) 9.43 (s, 1H), 8.20 (s, 1H), 7.85 (s, 1H), 7.28 (s, 1H), 6.05 (s, 1H), 5.97 (s, 1H), 5.41 (s, 3H), 4.86 (s, 2H).

Synthesis of PU: PU with different proportions of PPG (7.186, 7.131, 7.08, and 7.03 g), HDI (0.348, 0.285, 0.225, and 0.168 g), and THDI (0.466, 0.584, 0.694, and 0.800 g) were prepared with a similar protocol to the PU and they correspond to different *f* values. Typically, mix PPG and HDI and stir for 1 min, then add THDI and stir for half a minute, and finally add DBTDL and stir for 5 s, then pour into the mold and put it into the oven at 60 °C for 12 h.

Synthesis of ILs Polymeric Networks: One gram of [HVIm][PF_6] and 0.01 g of crosslinker [AVIm][PF_6] were mixed and stirred thoroughly, then 5 mg of Irgacure 1173 was added and left to cure completely under 365 nm light for 5 min.

Preparation of IL solution: Two grams [HVIm][PF_6], 0.02 g [AVIm][PF_6], 10 mg of Irgacure 1173, and 1 mg of Rhodamine were added to 2 g of dichloromethane and mix well.

Preparation of PILs-Interpenetrated PU: A brush dipped in ILS was drawn on the PU and left at 30 °C for 6 h to allow the dichloromethane to fully penetrate, then placed in a vacuum oven at 80 °C for 24 h to allow for the evaporation of the dichloromethane, and then taken out and polymerized under the irradiation of 365 nm light for 1 min.

Swelling of PU in ILS and the Volatilization of Dichloromethane: PU sheets with a thickness of ≈3 mm and a side length of ≈8 mm were immersed in ILS and weighed every 2 h. After the weight was stable, place

them in a vacuum oven at 80 °C, weigh them every 2 h, and then stop when the weight was stable.

Wear Resistance Evaluation: After wiping the surface of the PILs-interpenetrated PU, it is fixed under a 500 g weight, which is placed on sandpaper (400 mesh) and dragged to 30 cm for 10 cycles. The resistance after each abrasion is measured.

Tape Peeling Test: Put the 3 M tape (3 M 810) on the surface of PU, use 500 g weight to press on it, and wait for 1 min, then tear off the tape, and measure the resistance of PU.

Humidity Response Test: The different RH conditions (43%–98%) were achieved with different saturated salt solutions (K_2CO_3: 43%; NaBr: 59%; NaCl: 75%). The ionic circuits were placed close to the liquid surface at a constant distance to guarantee data accuracy during the experiment.[39]

Waterproofness Experiments: The surface of ionic PILs-interpenetrated PU was wiped clean, immersed the PU in deionized water for 12 h, then placed in a vortex mixer and shocked continuously for 8 h at 2500 rpm. Measure its resistance every 2 h. Similarly, the PILs-interpenetrated PU was immersed in a glass bottle containing deionized water, stirred continuously for 8 h, and measured its resistance every 2 h.

Measurements of Nyquist Plots: The Nyquist plots were obtained by an electrochemical workstation CHI 760 (Shanghai CH Instrument Co., Ltd., China) at a frequency of 10^4–1 Hz and an amplitude of 5 mV.

Preparation of Ionic Network: A customized stamp with a grid pattern was dipped into the ILS and printed on the PU substrate and the lines were traced repeatedly with a paintbrush. After 48 h of standing at 25 °C it was placed in a vacuum oven at 80 °C for 24 h, and then polymerized with 365 nm light for 10 min.

Circuit Connection of Ionic Network: Connect six adjacent endpoints in the ionic network to the positive electrodes of the electrochemical workstation and the other six endpoints to the negative electrodes. The electrochemical workstation monitors the resistance values between each positive and negative electrode.

Measurements and Characterization: Stress–strain curves of PU were conducted on a universal mechanical tester (Instron LEGEND 2367). Waterproofness Experiments were carried out by a vortex mixer (IKA MS3 Digital, Germany). The fluorescent microscope images were captured by a fluorescent microscope (Leica DMi8, Germany). ^{1}H NMR spectra were obtained from a Bruker 400 MHz spectrometer (Germany). Fourier transform infrared (FT-IR) spectra were recorded on a Bruker Tensor 27 spectrometer (Germany). A scanning electron microscope (SEM, Hitachi SU8010, Japan) was used to observe the cross section of the ionic circuit and the cross section of the distribution of elements. Pressure is applied, monitored, and controlled through a dynamometer (Series 5) and electric console (ESM 301, MARK-10, USA). ILS was printed with an inkjet printer (MicroFab Inkjet, Ruidu, Shanghai, China). Electrical responses of PILs-interpenetrated PU and ICN were recorded on a CHI 760 electrochemical workstation (Shanghai CH Instrument Co., Ltd., China).

Supporting Information

Supporting Information is available from the Wiley Online Library or from the author.

Acknowledgements

Y.A. and J.W. contributed equally to this work. This work was financially supported by the Beijing Natural Science Foundation (No. 2242037) and the National Natural Science Foundation of China (No. 22005336, 22475236). The authors would like to thank Dr. Zhiwu Chen for his helpful guidance on the operation of AC impedance and data processing. The authors also would like to thank Prof. Li Guan for her helpful guidance on the operation of EDS.

Conflict of Interest

The authors declare no conflict of interest.

Data Availability Statement

The data that support the findings of this study are available from the corresponding author upon reasonable request.

Keywords

direct ionic ink writing, interpenetrating network, patternable ionic circuit, waterproof, wear-resistant

Received: July 26, 2024
Revised: September 4, 2024
Published online:

[1] T. Wang, M. Wang, J. Wang, L. Yang, X. Ren, G. Song, S. Chen, Y. Yuan, R. Liu, L. Pan, Z. Li, W. R. Leow, Y. Luo, S. Ji, Z. Cui, K. He, F. Zhang, F. Lv, Y. Tian, K. Cai, B. Yang, J. Niu, H. Zou, S. Liu, G. Xu, X. Fan, B. Hu, X. J. Loh, L. Wang, X. Chen, *Nat. Electron.* **2022**, *5*, 586.
[2] J. Sun, C. Keplinger, G. M. Whitesides, Z. Suo, *Adv. Mater.* **2014**, *26*, 7608.
[3] C. Yang, Z. Suo, *Nat. Rev. Mater.* **2018**, *3*, 125.
[4] B. Chen, J. J. Lu, C. H. Yang, J. H. Yang, J. Zhou, Y. M. Chen, Z. Suo, *ACS Appl. Mater. Interfaces* **2014**, *6*, 7840.
[5] Z. Yu, P. Wu, *Adv. Mater.* **2021**, *33*, 2008479.
[6] S. Zhao, P. Tseng, J. Grasman, Y. Wang, W. Li, B. Napier, B. Yavuz, Y. Chen, L. Howell, J. Rincon, F. G. Omenetto, D. L. Kaplan, *Adv. Mater.* **2018**, *30*, 1800598.
[7] Y. An, Z. Yang, Y. Yang, X. Li, X. Zheng, Z. Chen, X. Wu, B. Xu, Y. Wang, Y. He, *Small* **2024**, *20*, 2308875.
[8] B. Park, J. H. Shin, J. Ok, S. Park, W. Jung, C. Jeong, S. Choy, Y. J. Jo, T. Kim, *Science* **2022**, *376*, 624.
[9] Y. Yang, Y. An, Z. Yang, B. Fu, Z. Chen, X. Zheng, B. Xu, W. Shen, Y. Wang, Y. He, *ACS Appl. Mater. Interfaces* **2023**, *15*, 23749.
[10] N. Gao, C. Pan, *SmartMat* **2024**, *5*, e1215.
[11] H. Lu, Y. Zhang, M. Zhu, S. Li, H. Liang, P. Bi, S. Wang, H. Wang, L. Gan, X.-E. Wu, Y. Zhang, *Nat. Commun.* **2024**, *15*, 3289.
[12] X. Cao, C. Ye, L. Cao, Y. Shan, J. Ren, S. Ling, *Adv. Mater.* **2023**, *35*, 2300447.
[13] Y. He, Q. Gui, S. Liao, H. Jia, Y. Wang, *Adv. Mater. Technol.* **2016**, *1*, 1600170.
[14] S. Zheng, W. Li, Y. Ren, Z. Liu, X. Zou, Y. Hu, J. Guo, Z. Sun, F. Yan, *Adv. Mater.* **2022**, *34*, 2106570.
[15] J. Li, D. Li, *ACS Appl. Mater. Interfaces* **2021**, *13*, 48208.
[16] Y. Zhong, G. T. M. Nguyen, C. Plesse, F. Vidal, E. W. H. Jager, *ACS Appl. Mater. Interfaces* **2018**, *10*, 21601.
[17] D. Won, H. Kim, J. Kim, H. Kim, M. W. Kim, J. Ahn, K. Min, Y. Lee, S. Hong, J. Choi, C.-Y. Kim, T.-S. Kim, S. H. Ko, *Nat. Electron.* **2024**, *7*, 475.
[18] J. Jia, H. Liu, S. Liao, K. Liu, Y. Wang, *Nano Lett.* **2022**, *22*, 9122.
[19] P. Li, J. Liu, J.-H. Yuan, Y. Guo, S. Wang, P. Zhang, W. Wang, *Nano Lett.* **2024**, *24*, 6192.
[20] H. Liu, D. Liu, J. Yang, H. Gao, Y. Wu, *Small* **2023**, *19*, 2206938.
[21] Z. Yuan, G. Shen, *Mater. Today* **2023**, *64*, 165.
[22] H. Wang, W. Wang, Z. Xie, *J. Polym Sci.* **2022**, *60*, 2679.
[23] H. C. Yu, X. P. Hao, C. W. Zhang, S. Y. Zheng, M. Du, S. Liang, Z. L. Wu, Q. Zheng, *Small* **2021**, *17*, 2103836.
[24] H. C. Yu, X. P. Hao, C. W. Zhang, S. Y. Zheng, M. Du, S. Liang, Z. L. Wu, Q. Zheng, *Small* **2021**, *17*, 2103836.
[25] D. Chen, C. Ni, L. Xie, Y. Li, S. Deng, Q. Zhao, T. Xie, *Sci. Adv.* **2021**, *7*, eabi7360.
[26] Z. Yang, Y. An, Y. He, X. Lian, Y. Wang, *Adv. Mater.* **2023**, *35*, 2303805.

[27] Z. Wang, L. Chen, Y. Chen, P. Liu, H. Duan, P. Cheng, *Research* **2020**, *2020*, 1426078.
[28] C. Zhang, H. Zheng, J. Sun, Y. Zhou, W. Xu, Y. Dai, J. Mo, Z. Wang, *Adv. Mater.* **2022**, *34*, 2105996.
[29] G. Ge, Q. Wang, Y. Zhang, H. N. Alshareef, X. Dong, *Adv. Funct. Mater.* **2021**, *31*, 2107437.
[30] Y. Miao, M. Xu, L. Zhang, *Adv. Mater.* **2021**, *33*, 2102308.
[31] S. Wu, Z. Zhao, J. R. Rzasa, E. Kim, J. Li, E. VanArsdale, W. E. Bentley, X. Shi, G. F. Payne, *Adv. Funct. Mater.* **2021**, *31*, 2007709.
[32] W. Gu, W. Li, Y. Zhang, Y. Xia, Q. Wang, W. Wang, P. Liu, X. Yu, H. He, C. Liang, Y. Ban, C. Mi, S. Yang, W. Liu, M. Cui, X. Deng, Z. Wang, Y. Zhang, *Nat. Commun.* **2023**, *14*, 5953.
[33] Z. Wu, Q. Ding, H. Wang, J. Ye, Y. Luo, J. Yu, R. Zhan, H. Zhang, K. Tao, C. Liu, J. Wu, *Adv. Funct. Mater.* **2024**, *34*, 2308280.
[34] B. Xu, Y. An, X. Zheng, Z. Chen, Z. Yang, Y. Yang, A. Zhang, Y. Wang, Y. He, *J. Mater. Chem. A* **2023**, *11*, 26617.
[35] R. Ludwig, *ChemSusChem* **2008**, *1*, 863.
[36] B. Zhao, J. Yan, F. Long, W. Qiu, G. Meng, Z. Zeng, H. Huang, H. Wang, N. Lin, X. Liu, *Adv. Sci.* **2023**, *10*, 2300857.
[37] H.-T. Cheng, L. Koc, J. Harmsen, T. Shaked, T. Chandra, H. Aradhye, G. Anderson, G. Corrado, W. Chai, M. Ispir, R. Anil, Z. Haque, L. Hong, V. Jain, X. Liu, H. Shah, In Proc. 1st workshop on deep learning for recommender systems, ACM, New York **2016**, 7.
[38] P. Wasserscheid, T. Welton, *Ionic Liquids in Synthesis*, Wiley, Weinheim, BW **2008**.
[39] C. Cai, C. Wen, W. Zhao, S. Tian, Y. Long, X. Zhang, X. Sui, L. Zhang, J. Yang, *ACS Appl. Mater. Interfaces* **2022**, *14*, 23692.